npj | 2D Materials and Applications

www.nature.com/npj2dmaterials

ARTICLE OPEN

Hypochlorite degrades 2D graphene oxide sheets faster than 1D oxidised carbon nanotubes and nanohorns

Leon Newman[1], Neus Lozano[1], Minfang Zhang[2], Sumio Iijima[2], Masako Yudasaka[2], Cyrill Bussy[1] and Kostas Kostarelos[1]

Carbon nanostructures are currently fuelling a revolution in science and technology in areas ranging from aerospace engineering to electronics. Oxidised carbon nanomaterials, such as graphene oxide, exhibit dramatically improved water dispersibility compared to their pristine equivalents, allowing their exploration in biology and medicine. Concomitant with these potential healthcare applications, the issue of degradability has been raised and has started to be investigated. The aim of the present study was to assess the potential of hypochlorite, a naturally occurring and industrially used ion, to degrade oxidised carbon nanomaterials within a week. Our main focus was to characterise the physical and chemical changes that occur during degradation of graphene oxide compared to two other oxidised carbon nanomaterials, namely carbon nanotubes and carbon nanohorns. The kinetics of degradation were closely monitored over a week using a battery of techniques including visual observation, UV–Vis spectroscopy, Raman spectroscopy, infra-red spectroscopy, transmission electron microscopy and atomic force microscopy. Graphene oxide was rapidly degraded into a dominantly amorphous structure lacking the characteristic Raman signature and microscopic morphology. Oxidised carbon nanotubes underwent degradation via a wall exfoliation mechanism, yet maintained a large fraction of the sp^2 carbon backbone, while the degradation of oxidised carbon nanohorns was somewhat intermediate. The present study shows the timeline of physical and chemical alterations of oxidised carbon nanomaterials, demonstrating a faster degradation of 2D graphene oxide sheets compared to 1D oxidised carbon nanomaterials over 7 days in the presence of an oxidising species.

npj 2D Materials and Applications (2017)1:39 ; doi:10.1038/s41699-017-0041-3

INTRODUCTION

Graphene is a two dimensional sp^2 carbon-based material that has acquired the attention and focus of experts from a myriad of disciplines. This comes following the revelation of its exceptional electronic,[1] mechanical,[2] thermal[3] and optical properties.[4] Among the various derivatives of graphene, graphene oxide (GO)[5] has demonstrated tremendous utility in water-based environments, since it surmounts one of graphene's caveats for its application in biomedicine, which is hydrophobicity. As of late, there are increasing proof-of-concept studies exploring the applicability of GO for biomedical use in comparison to other sp^2 hybridised carbon nanomaterials (CNMs), the body being predominantly a hydrophilic environment. For example, the delivery for both drug and diagnostic molecules,[6] the capturing of circulating cancer cells,[7] and the photo-thermal ablation of cancers.[8] Other studies have proposed the use of GO for its antibacterial properties[9] or as scaffolds in tissue engineering.[10] Looking less at the biomedical applicability and more at everyday applications, studies have demonstrated GO usage, in its reduced form, in paints as a means to prevent metal corrosion[11] or as molecular sieves in water filtration systems for desalination.[12] Overall these studies demonstrate the potential for wide use of GO in many commercial products.

One of the necessities for the introduction of a new material for industrial, medical or lay use is to understand its fate over time and therefore its potential degradability, for example, in the event of an intentional or unintentional release into the environment or human exposure. In relation to the toxicological consequences of CNMs, such as graphene, on living organisms there are still inconclusive results.[13] Some studies suggest the ability of graphene, for example, to penetrate cell membranes and potentially damage the cell interior,[14] while others report biocompatibility.[15] Further studies are therefore warranted in this area to conclude on the toxicological profile of CNMs. Regarding degradability, several studies have investigated and demonstrated the degradation of CNMs including graphene using enzymes, such as lignin peroxidase[16] or horseradish peroxidase.[17] Chemical strategies such as Fenton-based chemistry have also been tested.[18] However, studies directly comparing the degradation kinetics of CNMs of different geometries in an oxidative environment are lacking.

In this study, we aimed to further the current understanding of the fate of oxidised CNMs in an oxidative environment. We tested whether sodium hypochlorite (NaClO), colloquially known as bleach, was able to efficiently degrade GO flakes in suspension. Comparing the chemical degradation of GO to that of two other oxidised CNMs, specifically carbon nanohorns (OxNH) and oxidised multiwall carbon nanotubes (OxMWNT), we reasoned that GO will degrade faster than the other two nanomaterials due to its unique physicochemical features. NaClO was chosen since it is a commonly used chemical by the public and industry. Moreover, hypochlorite (ClO^-) is naturally produced in the human body by various enzymes, such as myeloperoxidase and eosinophil peroxidase.[19] It was our hypothesis that the strong

[1]Nanomedicine Laboratory, Faculty of Biology, Medicine and Health and National Graphene Institute, University of Manchester, AV Hill Building, Manchester M13 9PT, United Kingdom and [2]Institute of Advanced Science and Industrial Technology (AIST), Tsukuba, Ibaraki 305-8565, Japan
Correspondence: Cyrill Bussy (cyrill.bussy@manchester.ac.uk) or Kostas Kostarelos (kostas.kostarelos@manchester.ac.uk)

Received: 22 November 2016 Revised: 8 September 2017 Accepted: 17 October 2017
Published online: 08 November 2017

oxidative action of ClO^-, from NaClO, would induce oxidative damage to the graphitic backbone, ultimately degrading the nanostructures to various extents. The degradation processes mediated by ClO^- were followed over a week using a battery of characterisation methods. These included visual observation, transmission electron microscopy (TEM), atomic force microscopy (AFM), Raman spectroscopy, UV–Vis spectroscopy and Fourier transform infra-red spectroscopy (FT-IR). The observations were compared against when the materials were incubated in water. We found that incubation in NaClO induced severe structural modifications in GO that was consistent with the materials degradation. Over the course of a week, GO degraded more rapidly than OxNH or OxMWNT. The results of this study adds information to ratify a proposal we made in a previous report concerning the mechanism by which carbon-based nanomaterials may degrade under a strong oxidative environment.[13,20]

RESULTS

Figure 1 shows the characterisation of the as synthesised GO, OxMWNT and OxNH. The Raman spectra obtained demonstrate an enhanced scattering intensity in the D band relative to the G band, indicative of the presence of defects, expected as the materials were oxidised. AFM images show an average height of 2.3 ± 1.1 nm, 35.2 ± 5.0 nm and 65 ± 10 nm for GO, OxMWNT and OxNH structures, respectively. The average lateral dimensions (taken in the longest dimensions were determined from AFM analyses) of GO, OxMWNT and OxNH were shown to be 900 ± 500 nm, 800 ± 200 nm and 125 ± 35 nm. TEM imaging evidenced the characteristic shapes of the nanomaterials and confirms the dimensions indicated by AFM. The X-ray photoelectron spectroscopy (XPS) and thermogravimetric analysis (TGA; Supplementary Fig. S2) in a combinatory fashion confirmed that all three nanomaterials contained oxygen functionalities.

Figure 2 shows optical images (Fig. 2a) and UV–Vis absorbance at 700 nm (Fig. 2b). Images show how the visible colour of the dispersions of GO, OxMWNT and OxNH in H_2O and NaClO 1% vary over 7 days. Only the dispersions containing CNMs in NaClO 1% demonstrated a change in colour. This was true for all of the CNMs but more so for GO and OxMWNT, with OxNH only showing a modest increase of transparency by Day 7. For CNMs that were dispersed in H_2O, the contrary was true, no decrease in colour was apparent. UV–Vis spectroscopy demonstrated a decrease in absorbance at 700 nm over time for OxMWNT and OxNH when dispersed in NaClO 1% (Fig. 2b). Interestingly, the absorption signal decreased at a greater rate for OxMWNT than for OxNH and did not proceed to reduce further than the value obtained at Day 5. The signal for GO did not show absorption in this region. Moreover, it was not possible to infer information from the characteristic absorption peak at 230 nm due to interference by the NaClO components.[21] The absorption of all CNMs placed in H_2O, did not differ during the course of the experiment, indicating their maintenance. Spectra showing absorption between 400–800 nm are given in Supplementary Fig. S3.

Raman spectroscopy was employed to yield quantifiable data regarding the structural perturbations in the CNMs when incubated in NaClO 1%. Figure 3 shows the evolution of the Raman spectra of GO over time in H_2O (Fig. 3a) and NaClO 1% (Fig. 3b). At Day 0 in NaClO 1%, it is clear that characteristic scattering in the D and G bands are present in the Raman spectra of all investigated CNMs. Raman scattering peaks were observed in the region of the D and G bands present at ~1330 cm^{-1} and ~1590 cm^{-1} respectively for all three nanomaterials indicating their graphitic backbone. The positions of these scattering peaks remained constant, however their relative intensities altered over time. The D band scattering intensity appears to increase relative to that of the G band for all materials although to different extents as seen in Fig. 3c. By Day 3 and Day 5 for GO and OxNH respectively, the ratio of the scattering intensity in the D relative to the G bands (I_D/I_G) decreased (Fig. 3c). For OxMWNT however, the characteristic features remained intact, although with a progressively increasing I_D/I_G ratio. The corresponding spectra of CNMs dispersed in H_2O are shown in Supplementary Figs. S6-S8.

Figure 4 shows the ultra-structural changes in the CNMs over time when incubated in NaClO 1%, as followed by TEM. It is evident from the representative images of GO, OxMWNT and OxNH that each nanomaterial underwent gross structural and morphological changes, that were progressive over the course of the 7 days incubation in NaClO 1%. Images of the corresponding CNMs when dispersed in H_2O are displayed in Supplementary Fig. S4. AFM was used to provide corroborative evidence of the changes in the different CNMs structural and morphology when incubated in NaClO 1% (Fig. 4). They evidenced similar changes to that shown via TEM. An imaging area of 4 μm^2 was chosen in order to provide evidence of the ultra-structural changes that occurred over the course of the 7 days.

DISCUSSION

NaClO when placed in water results in the generation of ClO^- and sodium hydroxide (NaOH). ClO^- is a powerful oxidising agent. During an oxidation reaction, the ClO^- donates an oxygen atom and its electrons to the species to be oxidised. This releases the chloride ion (Cl^-). It is this process that allows NaClO to be used as an antimicrobial,[22] bleaching or strong oxidising agents. NaClO can also be used in chemical synthesis.[23] Nature too uses hypochlorous acid (HClO) and ClO^- for example in immune defence where it is produced by activated neutrophils and macrophages.[24] Within these cells, enzymes such as myeloperoxidase catalyse the conversion of H_2O_2 to $HClO/ClO^-$. These products are able to kill invading pathogens directly as well as modifying specific extracellular features[25,26] which can further promote the immune response allowing effective removal of invading pathogens.

With the recent surge of interest in the use of oxidised CNMs and the demonstration that these materials can undergo $HClO/ClO^-$ (from peroxidase enzymes)-mediated biodegradation,[19] it was our intention to use NaClO in water, hence ClO^-, in order to follow the oxidative degradation of different CNMs over a week. Previous studies have demonstrated the effect of ClO^- on carbon nanotubes.[27–30] The authors utilised the action of myeloperoxidase to convert H_2O_2 to ClO^-, which subsequently acted to oxidise the carbon nanotubes and ultimately degrade them. The oxidative action of ClO^- was confirmed, as aqueous NaClO was used as a positive control to degrade the CNMs. However, a direct comparison of the oxidative degradation kinetics of different CNMs is lacking. The specific objectives of the present study were therefore to assess the capacity of ClO^- to induce structural deformations on GO compared to two other oxidised CNMs, and to compare the structural changes and kinetics of decay. A concentration of NaClO 1% was selected as it is comparable to that used for house hold applications (3–6%) and also could degrade the materials at a rate that allowed us to follow the gradual structural changes that occurred in the nanomaterials over a week, as we determined through pilot studies.

To achieve our aims, a battery of characterisation techniques was employed. Characterisation of the starting oxidised CNMs revealed that all three nanomaterials were initially functionalised to a similar extent as indicated by TGA albeit with some differences with GO being the most and OxMWNT being the least functionalised (Supplementary Fig. S2). This trend was corroborated by the XPS data. Interestingly however, it appeared that the XPS results indicated that there was a slightly larger difference between the functionalisation of GO relative to the other two nanomaterials (Supplementary Fig. S1) than suggested by TGA. This may be because XPS is a surface technique that only

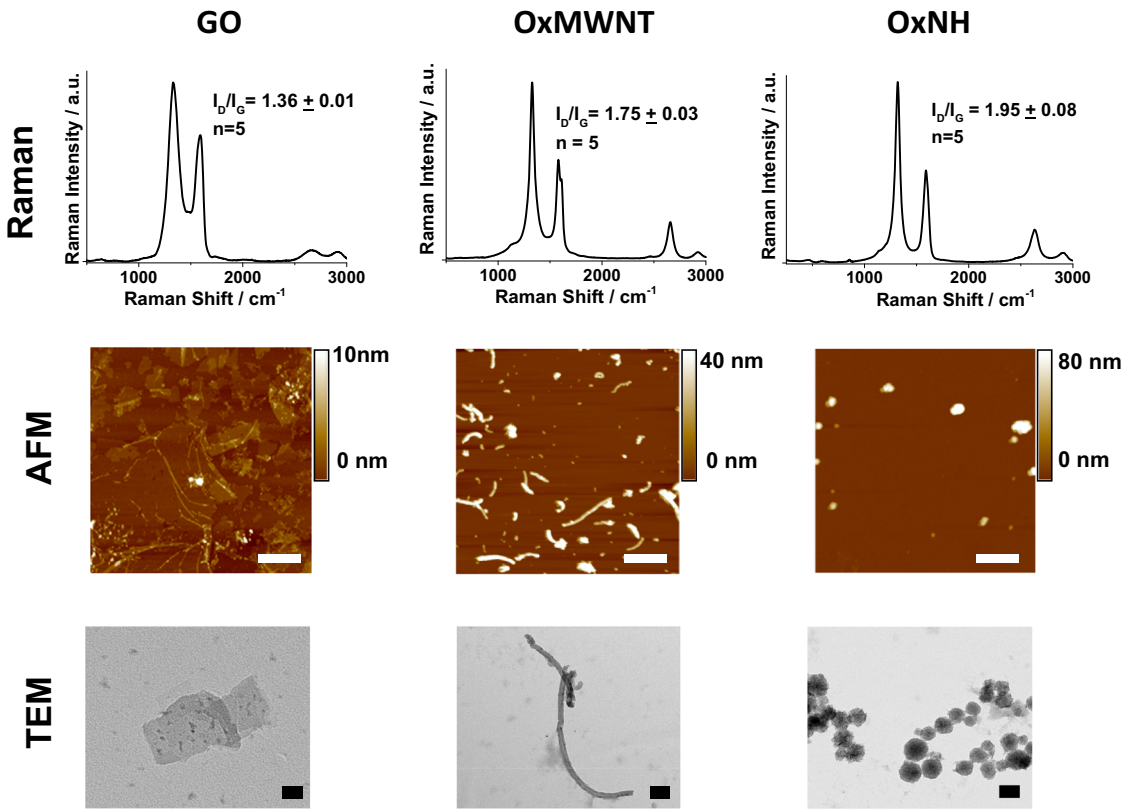

XPS

System	π-π*	O-C=O	C=O	C-O-C	C-OH	C-C&C=C	Total Functionalisation (%)
Graphite	289.9 eV	-	-	-	285.6 eV	284.6 eV	
	15.7%	-	-	-	19.2%	65.1%	19.2%
GO	290.8 eV	288.0 eV	286.8 eV	286.2 eV	-	284.6 eV	
	1.2%	16.2%	26.3%	19.2%	-	37.2%	61.7%
MWNT	289.7 eV	-	-	-	285.7 eV	284.6 eV	
	17.2%	-	-	-	20.5%	62.3%	20.5%
OxMWNT	-	-	287.2 eV	-	285.3 eV	284.6 eV	
	-	-	19.8%	-	22.4%	57.8%	42.2%
NH	289.3 eV	-	-	-	285.6 eV	284.6 eV	
	21.2%	-	-	-	27.1%	51.7%	27.1%
OxNH	-	288.2 eV	-	-	285.6 eV	284.6 eV	
	-	17.8%	-	-	24.4%	57.8%	42.2%

Fig. 1 Characterisation of the starting oxidised carbon nanomaterials. Carbon nanomaterials: graphene oxide (GO), oxidised multiwalled nanotubes (OxMWNT) and oxidised nanohorns (OxNH) were characterised by Raman spectroscopy to demonstrate the defected nature of the starting materials. AFM (scale bars = 500 nm) and TEM (scale bars = 100 nm) were utilised to allow visualisation of the nanomaterials and to indicate the dimensions of the materials. XPS was used to indicate the relative degree of oxygen functionalities on each of the nanostructures. XPS survey spectra and TGA are shown in the Supplementary Information (Supplementary Fig. S2)

allows a detailed regional surface analysis (analysis depth ≈ 10 nm),[31] as opposed to TGA which considers the entire sample structure allowing a more global analysis.[32] This is especially important when analysing OxMWNT and OxNH dahlia like structures, which have internal and external structural components, compared to 2D GO which does not. Despite these differences however, the results suggest that the overall functionalisation of all three materials was comparable. Interestingly and importantly, though the total functionalisation was comparable, the ratio of the specific surface oxygen functionalities differed between the respective nanostructures. GO contained a mixture of carboxylic acid, carbonyl and epoxide groups, whereas the OxMWNT contained carbonyl and hydroxyl groups, while OxNH was shown to contain carboxylic acid and hydroxyl groups. This may be a consequence of the starting nanomaterials dimensionality and also the means by which they were oxidised. It should be considered however, that the resolution of the C1s spectra was too low to allow for the deconvolution of hydroxyls from epoxides in GO. Nevertheless the GO is likely to also contain hydroxyl groups as per its FTIR spectra (Supplementary Fig. S9).

Other characterisation techniques used such as Raman spectroscopy (Fig. 1) demonstrated the presence of defects in the

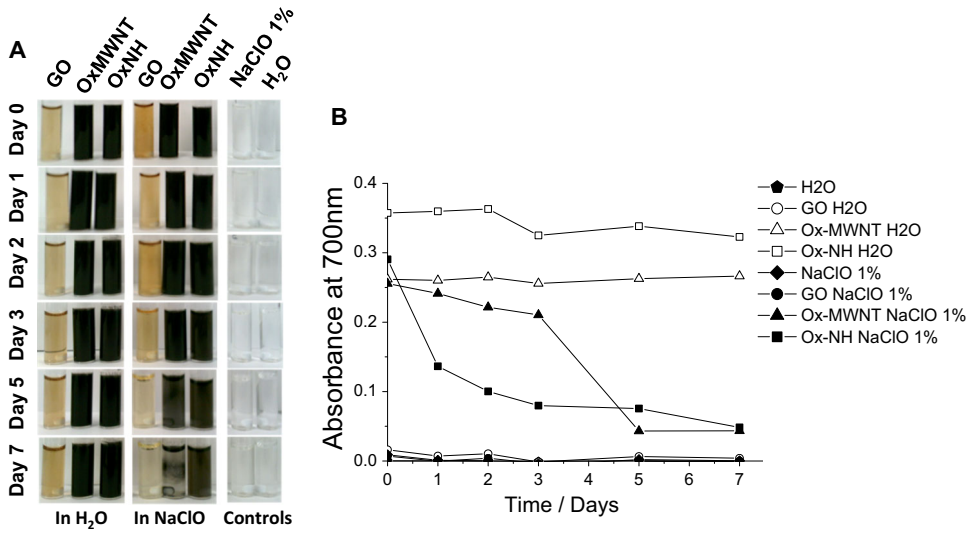

Fig. 2 Optical changes of oxidised carbon nanomaterials over time in NaClO 1%. **a** Visual appearance and colour of carbon nanomaterials in H_2O and in NaClO 1% at time points Day 0, 1, 2, 3, 5 and 7 are shown with controls: NaClO 1% and H_2O alone. The colour of oxidised carbon nanomaterials became less obvious over time when dispersed in NaClO 1% (samples were all repeated in triplicate). **b** UV–Vis was measured at 700 nm for all samples to indicate the degree of light absorption and scattering indicative of the physicochemical state of the dispersions. For OxMWNT and OxNH, there is a decrease in intensity at 700 nm

crystalline network of the starting materials as shown by an elevated D band scattering, which is expected following an oxidative reaction. The Raman spectral fingerprints obtained for the synthesised GO, OxMWNT and OxNH were comparable to that reported previously in the literature using identical or similar oxidation processes.[15,33]

To then monitor degradation, other characterisation techniques were used including visual observation (Fig. 2a) and UV–Vis absorption (Fig. 2b) to gain superficial information relating to the amount of material present in solution over time when the materials were incubated in NaClO 1%. It was interesting to observe that the GO dispersions were of a yellow/brown colour while the OxMWNT and OxNH had a black colouration. This has also been demonstrated by previous reports in the literature.[15,33] An explanation for the colouration is that during synthesis, the oxidation of the pristine graphite removes carbon atoms from participating in the extensive electron delocalisation present in graphene. This initially opens the band gap of the component graphene in the longer wavelength regions of the visible spectrum as a result of the reduction in electron delocalisation. Depending on the extent of oxidation, the band gap will continue to correspond to shorter wavelengths of light as the paths for electron delocalisation become increasingly limited due to further disruption of the π system. The lowest unoccupied C=C π electron states increase in energy as their abundance decreases, resulting in the change in colour from black graphene / graphite to orange-yellow GO dispersions.[34] The yellow brown colour cannot be seen obviously for OxMWNT and OxNH because of the denser structures, as well as lower degrees of oxidation in enclosed features such as the intact internal walls of OxMWNT, which may be oxidised to lesser extents. Following incubation in NaClO 1%, the intensities of the colours for each dispersion reduced in comparison to when the CNMs were incubated in water. This suggests a decrease in the presence of intact CNMs. On ceasing of magnetic stirring to image the contents in the reaction vessels, we noticed that the degrading OxMWNT gradually came out of solution to some extent over time, which never occurred prior to Day 3. This is potentially indicative of the decay of the outer walls and the revealing of more pristine and hydrophobic features of the inner walls. All other measurements were therefore completed following re-dispersion via pipetting to avoid inconsistent measurements.

UV–Vis spectra measurements were performed at 700 nm for all tested CNMs (Fig. 2b). We did not use the absorption maxima of the tested CNMs due to the interfering light absorption by the oxidative ClO^-.[21] Instead, we selected the 700 nm wavelength in order to measure simultaneously the light scattering and absorption by each material, as a means to spectroscopically evaluate the amount of materials present. For both OxMWNT and OxNH, there was a clear decrease of absorption and scattering overtime. This suggests a progressive but continuous degradation of both nanomaterials by ClO^-. The decrease in absorption and scattering by OxNH could be explained by a slow destruction of the starting dahlia-like shape as the individual nanohorns become progressively more oxidised. The decrease in scattering by OxMWNT was less regular, suggesting more complex degradation kinetics as previously discussed.[19,20] In contrast, no changes in absorption or scattering characteristics were observable for GO. Although useful for studying the patterns of CNM degradation, UV–Vis is not ideal for studying GO, especially in our case, where components of the ClO^- absorb near the GO absorption maximum[21] and no absorption or scattering is seen at longer wavelengths.

In order to obtain more conclusive quantifiable evidence of degradation, Raman spectroscopy was employed (Fig. 3a–c). All spectral intensities were normalised to the primary in plane vibrational mode peak intensity at 1590 cm^{-1} (G band). The value of the I_D/I_G ratio was then calculated. The D peak, present at ~1330 cm^{-1}, provided information about the abundance of defects.[35] As defects increase in the graphene plane, the D band scattering intensity will increase relative to the G band scattering intensity (I_D/I_G) and hence the degree of disorder can be rationalised.[36]

Over the first day, all the CNMs underwent an increase in I_D/I_G (Fig. 3c), indicative of the increasing degree of defects in the graphene planes due to oxidation by ClO^-. Similar observations were demonstrated in other CNM degradation studies.[17] Later on for GO, the I_D/I_G ratio began to decrease noticeably (Day 3) and the spectra started to lose the characteristic Raman signature of GO (Days 5 and 7). This was expected and is confirmation of degradation. As the disorder in the graphene-based sheet

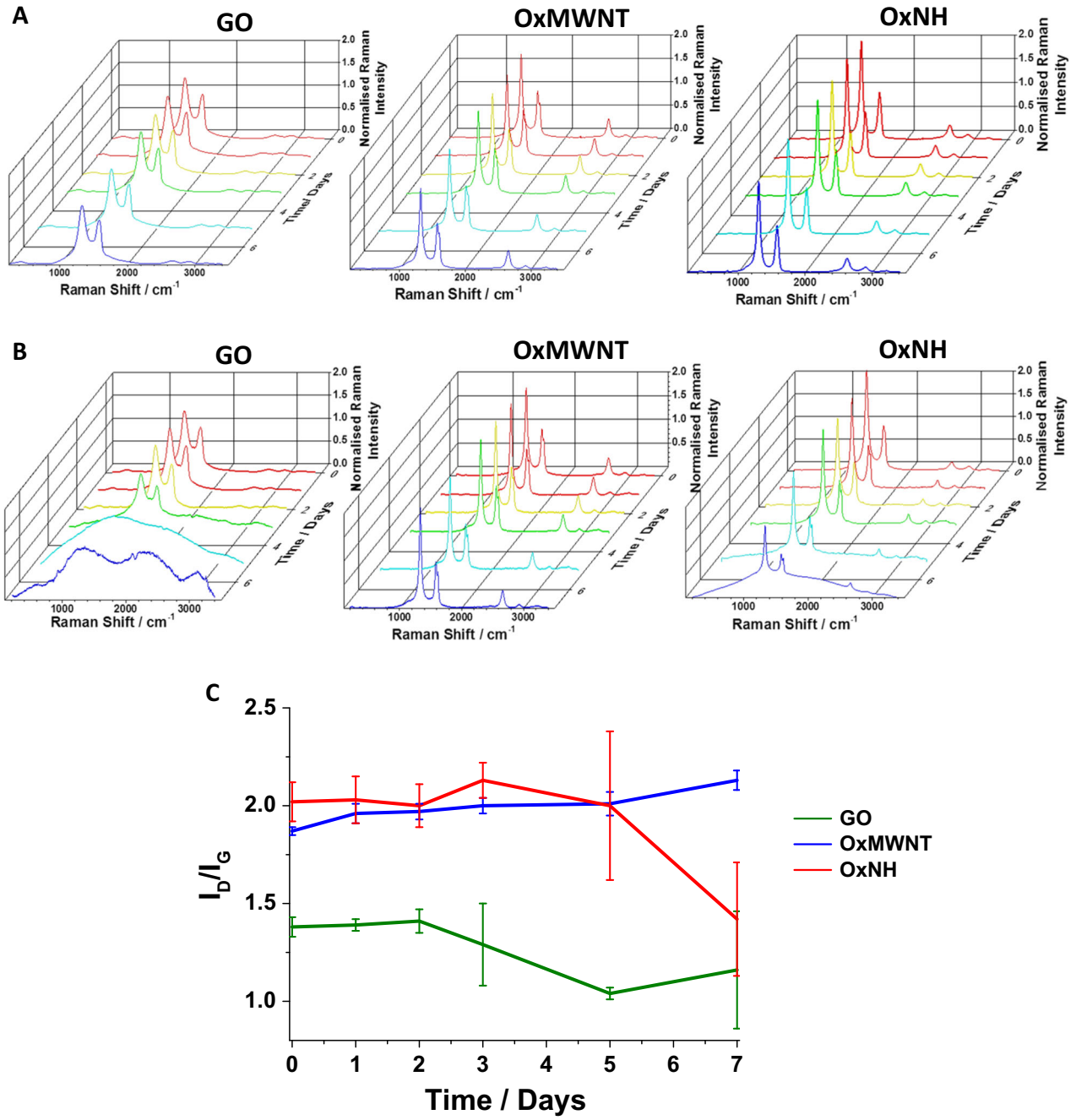

Fig. 3 Evolution of Raman spectra of oxidised carbon nanomaterials. The progressive changes in the spectral features of GO, OxMWNT and OxNH are shown at Days 0, 1, 2, 3, 5 and 7, when incubated in **a** H_2O and **b** NaClO 1%. At each time point the spectra is given in a different colour for clarity. **c** The average change in the I_D/I_G ratio over time for each CNM (GO—Green, OxMWNT—Blue and OxNH—Red) when incubated in NaClO 1% is given in C. Error bars have also been presented for each material in the respective colours at each time point ($n = 30$ measurements). All averaged individual Raman spectra have been presented in Supplementary Figs. S6-S8

increased, an initial rise in the I_D/I_G ratio was observed after 1 day as expected due to the increased scattering of charge carriers by defects and as the crystalline graphitic domains become smaller.[35,37] This however will occur only up to a certain defect density, above which the material would start to be described as nano-crystalline. Any more defects would result in an amorphisation of the sp^2 carbon structure, resulting in a reduction in the I_D/I_G ratio and subsequently an attenuation of all characteristic peaks, which is indicative of an increasing sp^3 amorphous carbon phase.[37]

A similar phenomenon (reduction in the I_D/I_G ratio) was seen for OxNHs after Day 5, which could be explained in the same manner. However OxNHs maintained some aspects of their characteristic Raman spectrum fingerprints even after 7 days, hence confirming that materials preserved some degree of their crystalline structure. In addition, the D′ peak at 1620 cm^{-1} was increasingly apparent over time for this material (Supplementary Fig. S8). Its appearance is further evidence of defect formation within the graphitic backbone.[38]

For OxMWNT, the D′ peak was already present in the materials Raman spectra at Day 0, and is a characteristic feature of the Raman spectra of these oxidised/defected materials. However, it was seen to increase with time (Supplementary Fig. S7),

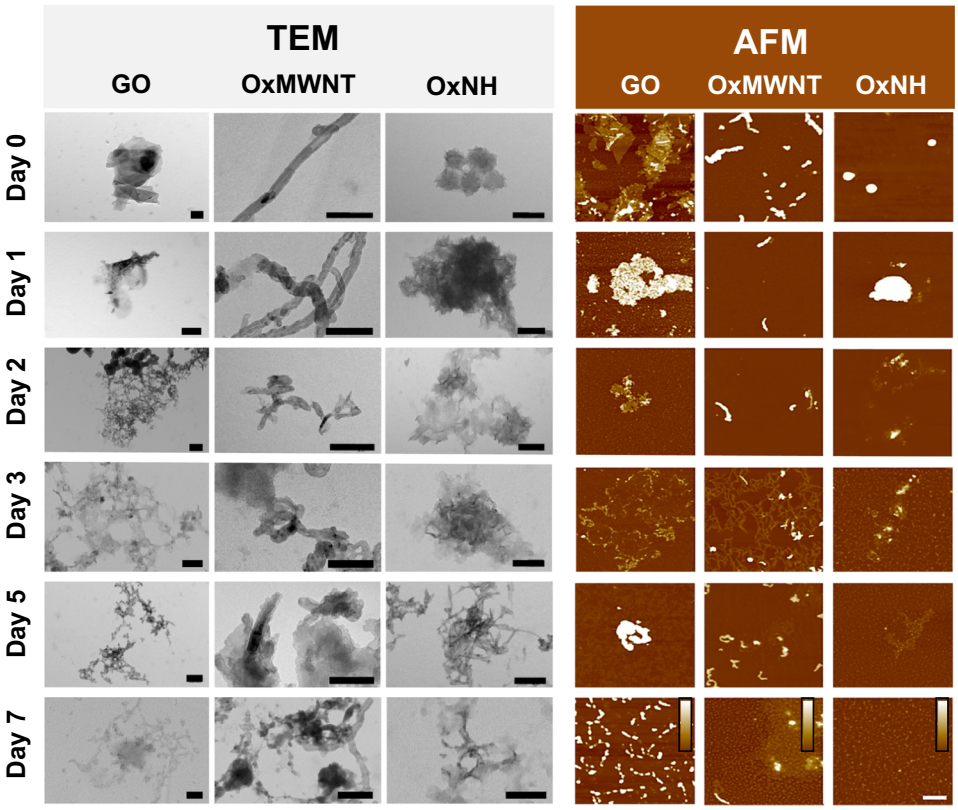

Fig. 4 Representative observations of ultra-structural changes in oxidised carbon nanomaterials exposed to NaClO 1% as detected by TEM (left) and AFM (right) over time. **a** Samples of GO, OxMWNT and OxNH were separated from NaClO salts via centrifugation at Days 0, 1, 2, 3, 5 and 7, and analysed via TEM (100 kV, scale bars = 100 nm) and AFM in tapping mode (lateral scale bars = 400 nm, height scale bars = 0–5 nm for GO, 0–20 nm for both OxMWNT and OxNH)

suggesting a further degradation when incubated with ClO^-.[38] The trend of the increasing then decreasing I_D/I_G ratio was less obvious relative to that seen for GO and OxNH. However, a pattern of increased (Days 0–1, 5–7) and then decreased (Day 1–5) gradient was seen (Fig. 3c), possibility due to the induction of nano-crystalline and amorphous carbon phases as consecutive graphene walls are exposed to the ClO^-. Previous studies conducted by us, when attempting to demonstrate the biodegradation of functionalised MWNT both in vivo[39] and in vitro[40] also showed an increase in the I_D/I_G ratios. The result was found when functionalised MWNT were internalised within microglia in the central nervous system. Others have also made similar observations.[29,41] These findings could be explained by the same mechanism, in which the outermost wall of the nanotubes gradually becomes dominated by amorphous structures following being subject to various oxidative degradation processes, which ultimately results in the nanotubes becoming gradually less intact.

Morphological analysis using TEM and AFM confirmed the structural degradation of all tested materials and showed patterns of degradation that were specific to each material (Fig. 4). For GO, the planar morphology was evident only up to Day 2. Interestingly after this time point, an increase in the sheet thickness was observed, most likely due to the increased presence of oxidation reaction by-products that adsorb to the GO sheet[18] following incubation in NaClO. After Day 2, the GO sheets were seen to contain holes and defects indicative of changes in the nano-crystalline state, as suggested by the Raman data. The material then became more amorphous with an unspecific morphology/3D structure which was eventually lost. These observations are similar to that reported previously when the horseradish peroxidase enzyme was incubated with H_2O_2 and GO.[17] The enzyme was able to bind to GO and induce structural defects by catalysing the conversion of H_2O_2 to stronger oxidative species. For OxMWNT and as expected, the degradation pattern was different with evident exfoliation of the OxMWNT outer walls at Days 5 and 7 (Supplementary Fig. S5). In our previous study on the biodegradation of functionalised MWNT, a similar observation was seen in the brains of animals.[39] Many other studies have observed similar TEM imaged features when MWNT are exposed to an oxidative influence.[42,43] But few have presented detailed imaging of the ultrastructural changes. For OxNH, the initial dahlia-like structure underwent a gross destruction indicative of the degradative capacity of ClO^-. Individualised nanohorns could be observed at Day 5 (Fig. 4). After this point, there was an increased presence of amorphous materials amongst remaining OxNH crystals as suggested by the Raman spectra (Fig. 3). Overall, the data suggest that NaClO is a substance with great capacity to degrade oxidised CNMs via further oxidation.

An explanation of why OxMWNT degraded at a slower rate than OxNH, is likely due to the intrinsic nature of the starting materials. Despite both being composed of rolled graphitic sheets with a hollow centre, the inner core of the NH (conical) is larger than in MWNT (tubular). This means that chemical reactions could more readily occur also from within the hollow centre of OxNH. In contrast, the inner hollow core of MWNTs is narrower and molecules entering, such as ClO^-, would be more constrained by the physical environment (i.e., the internal diameter of the innermost nanotube). In addition, the conical structure of OxNH is more irregular with opening of holes occurring on the side walls[44] allowing more accessibility for ClO^- molecules to reactive sites and for degradation to proceed. This is however not the case for OxMWNT, which maintains an inherently more crystalline non-defected structure within the internal enclosed walls. Finally, the closed and curved end of a single OxNH is more strained

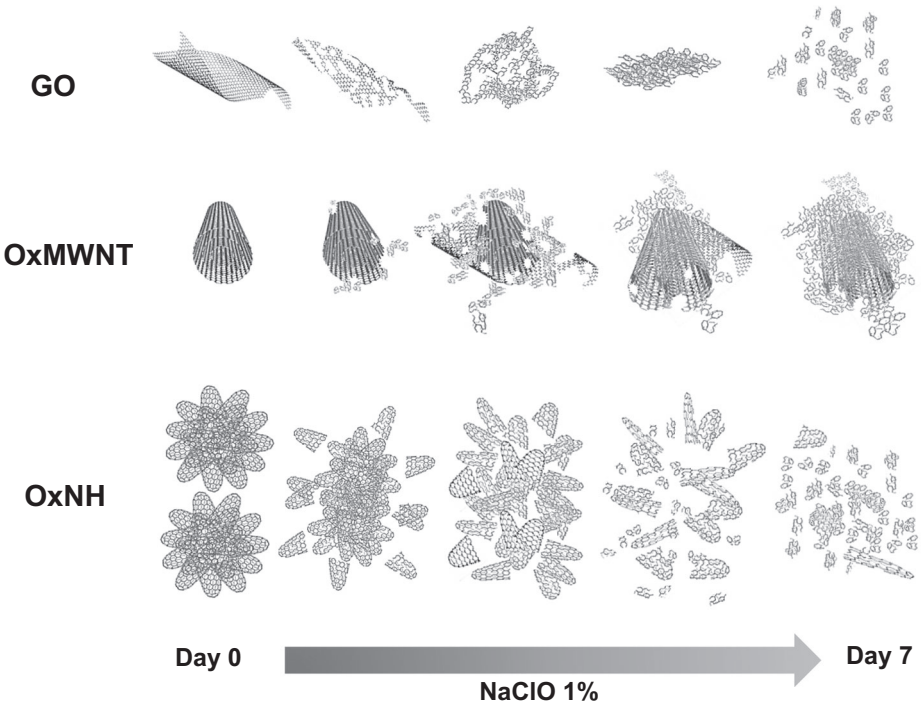

Fig. 5 Schematic representation of the degradation processes. The progressive decay in the structural integrity of **a** GO, **b** OxMWNT and **c** OxNH are shown over time following incubation in NaClO 1%

(pentagonal arrangements) and so more reactive[44] than the tips of a single OxMWNT (no caps, only edges). These factors are due to the unique geometry of the 1D CNMs and therefore are not relevant to GO, which exists as high surface area, planar 2D sheets.

In addition to the aspects of morphology, the identity of the prevailing surface functional groups for each CNM may be an important factor in driving the patterns and kinetics of degradation. This is due to the different relative stabilities and reactivities of epoxide, carbonyl and carboxylic acid functional groups towards reactive agents, such as ClO^-. For example, epoxide groups present in GO are particularly unstable and likely to react, due to the inductive effect of the oxygen and the unfavourable ring strain.[45] This may contribute to the observed hole formation (Fig. 4) in the GO sheets[16–18] where epoxides arise. Interestingly, ClO^- can form epoxides from alkene double bonds.[46] This could be a mechanism leading to the initial oxidation of the more poorly oxidised internal walls of OxMWNT, which will then go on to be further oxidised over time by ClO^-, leading to exfoliation (Supplementary Fig. S5). Hydroxyl and carbonyl groups can also react with ClO^-.[23,47,48] However carboxylic acid groups—the furthest state of oxidation of oxygen functionalities—are somewhat stabilised due to the delocalisation of the π electrons across the heteroatom. Nonetheless, carboxylic acid groups can react via oxidative decarboxylation reactions[49,50] essentially removing carbon and oxygen to form carbonates. The environment in which any functional groups are found can also influence both their stability and reactivity.

Degradation of CNMs via oxidative processes was further supported in our work by the dramatic changes between Day 0 and Day 7 in the FT-IR spectra for all nanomaterials incubated in NaClO 1% (Supplementary Fig. S9). After 7 days in NaClO, it was observed that the assignment bands related to C–O (1200–1000 cm^{-1}), C = O (~1726 cm^{-1}) and O–H vibrations (3500–3000 cm^{-1}) increased in intensity. Moreover, there was an increase in the aliphatic C–H stretch assignment band (2900–2800 cm^{-1}) suggesting an increase sp^3 C defective sites within the materials. These observations are in line with oxidative degradation. The Day 7 spectra were however most likely the result of a combination of spectra from materials still undergoing degradation and of spectra from an array of degradation by-products. The visually more translucent appearance of the material suspensions at Day 7 (Fig. 2a) was suggestive of the well-dispersed and the increasingly non-graphitic nature of the by-products.[29] The detailed mechanism of the molecular degradation process should however be further investigated to isolate and characterise these degradation by-products.

In this study, ClO^-, from NaClO, has been shown to completely degrade GO 2D sheets with rapid kinetics compared to 1D OxMWNT and OxNH, which did not occur when the materials were incubated in H_2O. Furthermore, detailed imaging of the morphological patterns by which oxidised CNM degrade has been provided. A summary schematic of the timeline and morphological degradation patterns for the various oxidised CNMs tested is proposed below (Fig. 5). Further studies are however required to isolate, identify and assess the environmental and biological impacts of the degradation by-products generated by ClO^- upon reaction with oxidised CNMs. As highlighted in other studies,[18] this is of particular importance since some of these degradation by-products could have chemical structures close to polyaromatic hydrocarbons, which are well-known carcinogenic molecules. Those experiments will help to complete the toxicological profile of these unique materials.

METHODS

Preparation of GO

The preparation of GO was based on a modified Hummers' method as described previously.[15] The concentration of the obtained GO product was 2.4 mg/mL and was adjusted to 2 mg/mL with MilliQ H_2O.

Preparation of OxMWNT

Pristine MWNT (1 g) (Nanoamor, USA) was sonicated in an ultrasonic cleaner (20 W, 40 kHz) (VWR, UK) for 24 h in 150 mL of sulphuric acid: nitric

acid (3:1) 98 and 65%, respectively at room temperature. Ice was added to reduce the temperature. The reaction mixture was added to H_2O to allow for a 10-fold dilution. The diluted mixture was filtered through a 0.45 µm Omnipore membrane filter (Merk, UK) and the OxMWNTs were suspended in MilliQ water, this was repeated until the pH was neutral. Samples were characterised as for GO.

Preparation of OxNH

OxNH were prepared as previously described.[30]

Incubation of oxidised CNMs with NaClO

Dispersions of oxidised CNMs were made up at 250 µg/mL with NaClO 1% (Sigma-Aldrich, UK) in glass vials to 3 mL and gently stirred using a magnetic stirrer at room temperature (pH 10), pH was monitored daily to ensure maintenance. Each reaction was completed thrice. At days 0, 1, 2, 3, 5 and 7 after incubation 160 µL were removed from each vessel, transferred to an Eppendorf tube and made up to 660 µL with MilliQ H_2O. The dispersion underwent centrifugation at 4000 rpm and the supernatant was discarded and replaced with 500 µL MilliQ water. This was repeated until the pH of the supernatant was neutral. This extracted material was then further analysed to monitor degradation. As controls, we used CNM dispersions (250 µg/mL) in MilliQ H_2O, MilliQ H_2O alone and 1% NaClO. These were treated in an identical manner.

Thermogravimetric analysis

Dried CNMs were placed in a crucible set at 25 °C in a TGA 400 thermogravimetric analyser (PerkinElmer, UK). The temperature was increased at 10 °C/min from 25–995 °C, under a nitrogen flow of 20 mL/min.

X-ray photoelectron spectroscopy

X-ray Photoelectron Spectroscopy was conducted (Thermo Scientific, UK) at the NEXUS facility (the UK's National EPSRC XPS Users' Service, hosted by NanoLAB in Newcastle-upon-Tyne). XPS was accomplished using a Thermo Theta Probe XPS spectrometer with a monochromatic Al K-α source of 1486.68 eV. The survey XPS spectra were acquired with pass energy (PE) of 200 eV, 1 eV step size, 50 ms dwell time and averaged over five scans, etching was set to 90 s. The high resolution C1s XPS spectra were acquired with PE of 40 eV, step size of 0.1 eV, dwell time of 100 ms and averaged over 20 scans. Spectra of insulating samples were charge corrected via shifting the peaks to the adventitious carbon C 1 s spectral component binding energy set to 284.6 eV. CasaXPS (Casa Software LTD, UK) remote software was used to analyse the spectra.

UV–Vis spectroscopy

Samples (1 mL) were analysed in 1.5-mL quartz cuvettes using a Varian Cary 50 spectrometer (Agilent Technologies, UK) and scanned between wavelengths of 200–800 nm.

Raman spectroscopy

Spectra were collected using a micro-Raman spectrometer (Thermo scientific, UK) with a laser, $\lambda = 633$ nm. Spectra were collected at a laser power of 0.4 mW (GO) and 0.8 mW (OxMWNT and OxNH) at a magnification of 50× with 25 s exposure time, averaged over 30 locations. Spectra were considered between 250–3500 cm^{-1}. The sample processing involved baseline subtraction and normalisation of the scattering intensity according to the G band scattering.

Transmission electron microscopy

Aliquots of the respective dispersions were transferred to 400-mesh copper grids with a support film of carbon (CF400-Cu) (EMS, UK). Excess dispersion was removed with filter paper. The specimens were examined using a FEI Tecnai 12 BioTwin TEM (FEI, Eindhoven, NL), using 100 kV electron beam. Images were captured by an AMT digital camera (Gatan, UK).

Atomic force microscopy

A multimode atomic force microscope (Bruker, UK) was applied in tapping mode. Using an Otespa tapping mode tip (Bruker, UK), scans were performed using the following parameters: a scan rate of 1 Hz, 512 lines per scan, an integral gain of 1 and a proportional gain of 5. Images were taken at 50, 20, 10, 5 and 2 µm (1:1 aspect ratio). Post image processing was completed using Bruker Nanoscope Analysis Version 1.4 (Bruker, UK).

Attenuated total reflectance FT-IR spectroscopy

Measurements were performed using a Tensor 27 FTIR machine (Bruker, UK) with a 3000 Series TM High Stability Temperature Controller with RS232 Control (Specac, UK) at 60 °C. Data processing was completed using OriginPro 8.5.1 software (Origin Lab, USA).

Data availability

The data sets generated during and/or analysed during the current study are available from the corresponding author on reasonable request.

ACKNOWLEDGEMENTS

The authors would like to thank the Engineering and Physical Sciences Research Council NowNano DTC program at the University of Manchester, UK (EP/G03737X/1; Leon Newman PhD studentship) and the FP7 EC Graphene Flagship project (FP7-ICT-2013-FET-F604391) for financially supporting this research. We thank Prof. Nicola Tirelli for kindly allowing the use of his FT-IR. We thank the staff in the Faculty of Biology, Medicine and Health EM Facility, Dr Aleksandr Mironov and Ms Samantha Forbes, for their expertise and the Wellcome Trust for equipment grant support to the Facility. The University of Manchester Bioimaging Facility microscopes used in this study were purchased with grants from the BBSRC, Wellcome Trust and the University of Manchester Strategic Fund. We thank Dr Nigel Hodson for his expert advice in the use of AFM and the NEXUS facility for the XPS service.

AUTHOR CONTRIBUTIONS

L.N, C.B. and K.K conceived the overall project. M.Z, S.I. and Y.M. produced, characterised and provided the starting carbon nanohorns. L.N. characterised the materials under degradation and analysed the data. All authors contributed toward the manuscript writing and approved of its content.

ADDITIONAL INFORMATION

Supplementary information accompanies the paper on the *npj 2D Materials and Applications* website (https://doi.org/10.1038/s41699-017-0041-3).

Competing interests: The authors declare that they have no competing financial interests.

Publisher's note: Springer Nature remains neutral with regard to jurisdictional claims in published maps and institutional affiliations.

REFERENCES

1. Novoselov, K. S. et al. Electric field effect in atomically thin carbon films. *Science* **306**, 666–669 (2004).
2. Lee, C., Wei, X., Kysar, J. W. & Hone, J. Measurement of the elastic properties and intrinsic strength of monolayer graphene. *Science* **321**, 385–388 (2008).
3. Balandin, A. A. Thermal properties of graphene and nanostructured carbon materials. *Nat. Mater.* **10**, 569–581 (2011).
4. Falkovsky, L. A. Optical properties of graphene. *J. Phys. Conf. Ser.* **129**, 012004 (2008).
5. Park, S. & Ruoff, R. S. Chemical methods for the production of graphenes. *Nat. Nanotech.* **4**, 217–224 (2009).
6. Sun, X. et al. Nano-graphene oxide for cellular imaging and drug delivery. *Nano Res.* **1**, 203–212 (2008).
7. Yoon, H. J. et al. Sensitive capture of circulating tumour cells by functionalized graphene oxide nanosheets. *Nat. Nanotechnol.* **8**, 735–741 (2013).
8. Robinson, J. T. et al. Ultrasmall reduced graphene oxide with high near-infrared absorbance for photothermal therapy. *J. Am. Chem. Soc.* **133**, 6825–6831 (2011).
9. Liu, S. et al. Antibacterial activity of graphite, graphite oxide, graphene oxide, and reduced graphene oxide: membrane and oxidative stress. *ACS Nano* **5**, 6971–6980 (2011).
10. Nishida, E. et al. Graphene oxide coating facilitates the bioactivity of scaffold material for tissue engineering. *Jpn. J. Appl. Phys.* **53**, 06JD04 (2014).
11. Su, Y. et al. Impermeable barrier films and protective coatings based on reduced graphene oxide. *Nat. Commun.* **5**, 4843 (2014).

12. Abraham, J. et al. Tunable sieving of ions using graphene oxide membranes. *Nat. Nanotech.* **12**, 546–550 (2017).
13. Kostarelos, K. & Novoselov, K. S. Materials science. Exploring the interface of graphene and biology. *Science* **344**, 261–263 (2014).
14. Li, Y. et al. Graphene microsheets enter cells through spontaneous membrane penetration at edge asperities and corner sites. *Proc. Natl. Acad. Sci. USA* **110**, 12295–12300 (2013).
15. Ali-Boucetta, H. et al. Graphene oxide: purified graphene oxide dispersions lack in vitro cytotoxicity and in vivo pathogenicity. *Adv. Healthcare Mater.* **2**, 512–512 (2013).
16. Lalwani, G., Xing, W. & Sitharaman, B. Enzymatic degradation of oxidized and reduced graphene nanoribbons by lignin peroxidase. *J. Mater. Chem. B* **2**, 6354–6362 (2014).
17. Kotchey, G. P. et al. The enzymatic oxidation of graphene oxide. *ACS Nano* **5**, 2098–2108 (2011).
18. Bai, H. et al. Insight into the Mechanism of graphene oxide degradation via the photo-Fenton reaction. *J. Phys. Chem. C* **118**, 10519–10529 (2014).
19. Kotchey, G. P. et al. A natural vanishing act: the enzyme-catalyzed degradation of carbon nanomaterials. *Acc. Chem. Res.* **45**, 1770–1781 (2012).
20. Bussy, C, Bianco, A, Prato, M. & Kostarelos, K. *Handbook of Safety Assessment of Nanomaterials: Toxicological Testing to Personalized Medicine* Ch. 11 (Pan Stanford Pub. Ltd., Stanford, 2014).
21. Zimmerman, G. & Strong, F. C. Equilibria and spectra of aqueous chlorine solutions. *J. Am. Chem. Soc.* **79**, 2063–2066 (1957).
22. Winter, J., Ilbert, M., Graf, P. C. F., Özcelik, D. & Jakob, U. Bleach activates a redox-regulated chaperone by oxidative protein unfolding. *Cell* **135**, 691–701 (2008).
23. Mirafzal, G. A. & Lozeva, A. M. Phase transfer catalyzed oxidation of alcohols with sodium hypochlorite. *Tetrahedron Lett.* **39**, 7263–7266 (1998).
24. Klebanoff, S. J. Myeloperoxidase: friend and foe. *J. Leukoc. Biol.* **77**, 598–625 (2005).
25. Malle, E., Marsche, G., Arnhold, J. & Davies, M. J. Modification of low-density lipoprotein by myeloperoxidase-derived oxidants and reagent hypochlorous acid. *Biochim. Biophys. Acta* **1761**, 392–415 (2006).
26. Hawkins, C. L. & Davies, M. J. Inactivation of protease inhibitors and lysozyme by hypochlorous acid: role of side-chain oxidation and protein unfolding in loss of biological function. *Chem. Res. Toxicol.* **18**, 1600–1610 (2005).
27. Vlasova, I. I., Sokolov, A. V., Chekanov, A. V., Kostevich, V. A. & Vasil'ev, V. B. Myeloperoxidase-induced biodegradation of single-walled carbon nanotubes is mediated by hypochlorite. *Bioorg. Khim.* **37**, 510–521 (2011).
28. Vlasova, I. I. et al. PEGylated single-walled carbon nanotubes activate neutrophils to increase production of hypochlorous acid, the oxidant capable of degrading nanotubes. *Toxicol. Appl. Pharmacol.* **264**, 131–142 (2012).
29. Kagan, V. E. et al. Carbon nanotubes degraded by neutrophil myeloperoxidase induce less pulmonary inflammation. *Nat. Nanotech.* **5**, 354–359 (2010).
30. Lu, N., Li, J., Tian, R. & Peng, Y. Y. Binding of human serum albumin to single-walled carbon nanotubes activated neutrophils to increase production of hypochlorous acid, the oxidant capable of degrading nanotubes. *Chem. Res. Toxicol.* **27**, 1070–1077 (2014).
31. Gorham, J. M. et al. Detecting carbon in carbon: exploiting differential charging to obtain information on the chemical identity and spatial location of carbon nanotube aggregates in composites by imaging x-ray photoelectron spectroscopy. *Carbon N. Y.* **96**, 1208–1216 (2016).
32. Charsley, E. L. & Warrington, S. B. *Compositional Analysis by Thermogravimetry* Ch. 2 (Astm Intl, Baltimore, 1988).
33. Zhang, M., Yudasaka, M., Ajima, K., Miyawaki, J. & Iijima, S. Light-assisted oxidation of single-wall carbon nanohorns for abundant creation of oxygenated groups that enable chemical modifications with proteins to enhance biocompatibility. *ACS Nano* **1**, 265–272 (2007).
34. Texter, J. Graphene dispersions. *Curr. Opin. Colloid Interface Sci.* **19**, 163–174 (2014).
35. Thomsen, C. & Reich, S. Double resonant Raman scattering in graphite. *Phys. Rev. Lett.* **85**, 5214–5217 (2000).
36. Childres, I, Jaureguib, L. A, Parkb, W, Caoa, H. & Chen, Y.P. *New Developments in Photon and Materials Research* Ch. 19 (Nova Science Pub. Inc., New York, 2013).
37. Lucchese, M. M. et al. Quantifying ion-induced defects and Raman relaxation length in graphene. *Carbon. N. Y.* **48**, 1592–1597 (2010).
38. Dresselhaus, M. S., Jorio, A., Hofmann, M., Dresselhaus, G. & Saito, R. Perspectives on carbon nanotubes and graphene raman spectroscopy. *Nano Lett.* **10**, 751–758 (2010).
39. Nunes, A. et al. In vivo degradation of functionalized carbon nanotubes after stereotactic administration in the brain cortex. *Nanomedicine (Lond).* **7**, 1485–1494 (2012).
40. Bussy, C., Hadad, C., Prato, M., Bianco, A. & Kostarelos, K. Intracellular degradation of chemically functionalized carbon nanotubes using a long-term primary microglial culture model. *Nanoscale* **8**, 590–601 (2016).
41. Elgrabli, D. et al. Intracellular degradation of functionalized carbon nanotube/iron oxide hybrids is modulated by iron via nrf2 pathway. *Sci. Rep.* **7**, 40997 (2017).
42. Russier, J. et al. Oxidative biodegradation of single - and multi-walled carbon nanotubes. *Nanoscale* **3**, 893–896 (2011).
43. Liu, X., Hurt, R. H. & Kane, A. B. Biodurability of single-walled carbon nanotubes depends on surface functionalization. *Carbon. N. Y.* **48**, 1961–1969 (2010).
44. Yudasaka, M, Iijima, S. & Crespi, V. H. *Carbon Nanotubes: Advanced Topics in the Synthesis, Structure, Properties and Applications* Ch. 19 (Springer-Verlag: Berlin, 2008).
45. Morgan, K. M. et al. Thermochemical studies of epoxides and related compounds. *J. Org. Chem.* **78**, 4303–4311 (2013).
46. de Poorter, B. & Meunier, B. Catalytic epoxidation of aliphatic terminal olefins with sodium hypochlorite. *Tetrahedron. Lett.* **25**, 1895–1896 (1984).
47. Khurana, J. M., Sharma, P., Gogia, A. & Kandpal, B. M. Oxidative cleavage of 1, 2-diols, α-ketols and 1, 2-diketones with aqueous sodium hypochlorite. *Org. Prep. Proc. Int.* **39**, 185–189 (2007).
48. Leduc, A. B. & Jamison, T. F. Continuous flow oxidation of alcohols and aldehydes utilizing bleach and catalytic tetrabutylammonium bromide. *Org. Process Res. Dev.* **16**, 1082–1089 (2012).
49. Whistler, R. L. & Yagi, K. Further Application of the hypochlorite method of chain shortening in the carbohydrate series1. *J. Org. Chem.* **26**, 1050–1052 (1961).
50. Elmore, P. R. et al. Hypochlorite-induced oxidative decarboxylation of trisubstituted acetic acids. *J. Org. Chem.* **54**, 970–972 (1989).